

Disorder Effects in Topological States Brief Review of the Recent Developments

Binglan Wu,¹ Juntao Song,² Jiaojiao Zhou,¹ and Hua Jiang^{1,*}

¹*College of Physics, Optoelectronics and Energy, Soochow University, Suzhou 215006, China*

²*Department of Physics, Hebei Normal University, Hebei 050024, China*

(Dated: November 30, 2017)

Disorder inevitably exists in realistic samples, manifesting itself in various exotic properties for the topological states. In this paper, we summarize and briefly review work completed over the last few years, including our own, regarding recent developments in several topics about disorder effects in topological states. For weak disorder, the robustness of topological states is demonstrated, especially for both quantum spin Hall states with $Z_2 = 1$ and size induced nontrivial topological insulators with $Z_2 = 0$. For moderate disorder, by increasing the randomness of both the impurity distribution and the impurity induced potential, the topological insulator states can be created from normal metallic or insulating states. These phenomena and their mechanisms are summarized. For strong disorder, the disorder causes a metal-insulator transition. Due to their topological nature, the phase diagrams are much richer in topological state systems. Finally, the trends in these areas of disorder research are discussed.

PACS numbers: 73.61.-r, 71.23.-b, 73.43.-f

I. INTRODUCTION

Topological states, including gapped topological insulators and gapless topological semimetals, have become a focus of the condensed matter research¹⁻⁸. In condensed matter systems, the first well-known insulating topological state is quantum Hall effect (QHE) under a strong magnetic field⁹. Subsequently, the quantum anomalous Hall effect (QAHE), a topological state similar as the QHE but without magnetic field, was proposed in 1988¹⁰ and observed in 2013¹¹. In 2005, Kane et al made a great step in the topological states research. They proposed the two-dimensional Z_2 topological insulator - quantum spin Hall effect (QSHE) in graphene, which extends the topological state into the class of systems protected by time reversal symmetry^{12,13}. Soon afterwards, the concept of symmetry protected topological states is broaden into three-dimension^{14,15} and other discrete symmetries^{7,16}. Besides the insulating systems, the topological states can also exist in gapless systems^{17,18}. More recently, topological semimetals, containing both Weyl semimetals and Dirac semimetals, were experimentally verified^{19,20}, soon after they were predicted in the corresponding materials^{21,22}. The topological states are different from normal metallic and insulating states because of the existence of nontrivial topological order, which originates from the global properties of all electrons below the Fermi energy²³ and can be characterized by various types of topological invariant numbers^{2,13,23}. Due to the nontrivial topological order, corresponding gapless states emerge on the surface, leading to numerous exotic properties in topological systems. These properties have been reviewed in references¹⁻⁸.

Experimentally, disorder is ubiquitous because of the defects in manufacturing processes and usually plays a dominant role in the transport properties of the samples being studied. Due to their unique electric structures, the response of topological states to disorder is fundamentally different from that in normal metals and insulators^{1,3,4,9,23-33}. Physically, the topological invariant number can take on only a few discrete values. Therefore, the topological order cannot be easily disrupted by weak perturbations. That is to say, quantized transport that is robust against weak disorder can be obtained in various of topological systems. Moreover, arising from their topological nature, topological states also show unconventional properties under moderate and strong disorder. Thus, studies of disorder effects can not only give a comprehensive understanding about topological states, but also offer a route map for the application of

topological states. In this paper, based on several of our finished works in the last few years^{30–33}, we briefly review three topics covered by recent studies of disorder effects in topological states. We note that there are other topics related to disorder, such as the weak anti-localization^{26,27}, the chiral anomaly effects^{28,29} etc, which are not reviewed here.

The rest of this paper is organized as follows. In Section 2, the robustness of topological states against weak disorder is reviewed. In section 3, we present how various type of disorder create topological insulator states from normal insulating or metallic states. In section 4, the main results from studies of the metal-insulator transition in topological states system are summarized. Finally, a brief conclusion and an outlook for future disorder research are given in Section 5.

II. ROBUSTNESS OF TOPOLOGICAL STATES

Searching for material states with low-power dissipation is one of the greatest challenges in modern fundamental physics and materials science. In a real experimental sample, disorder always exists to some degree. A carrier propagating inside the sample will inevitably collide with disorder sites and be scattered. However, whether such a collision can cause energy dissipation depends on the ability of the scattering to induce backscattering processes – carriers propagating in the forward channel are scattered into the backward channel. In a normal metal, due to the spatial overlap between the forward and backward channels, backscattering can occur even for weak disorder. Therefore, the resistance (conductance) in a normal metal is not universal but in general increases (decreases) with the disorder strength. Transport in such a system is dissipative. In sharp contrast, in various kinds of topological systems, the spatial separation between the forward and backward channels and the existence of a special discrete symmetry (e.g. time-reversal symmetry) forbid backscattering³⁴. As a result, carriers can propagate without dissipation. Thus, the resistance (conductance) in these systems is quantized and is insensitive to the presence of weak disorder. Such exotic phenomenon, namely the robustness of topological states, makes their host materials ideal platforms for testing fundamental physics principles and achieving low-power dissipation in electronic/spintronic devices.

That topological states are robust against weak disorder was first discovered in a milestone experiment on quantum Hall effects⁹. Klitzing et al observed quantized Hall resistance and zero longitudinal resistance, independent of the material details. Subsequently, such phenomena have been extensively studied both within the context of quantum Hall effect and in various other topological states^{35–41}. In the following, as examples, we demonstrate the robustness of the topological states and the mechanisms of this behavior in two recently discovered systems: (i) quantum spin Hall effects (QSHE) in HgTe/CdTe quantum wells³⁰ and (ii) new proposed $Z_2 = 0$ topological insulators with emerging robust helical surface states³¹.

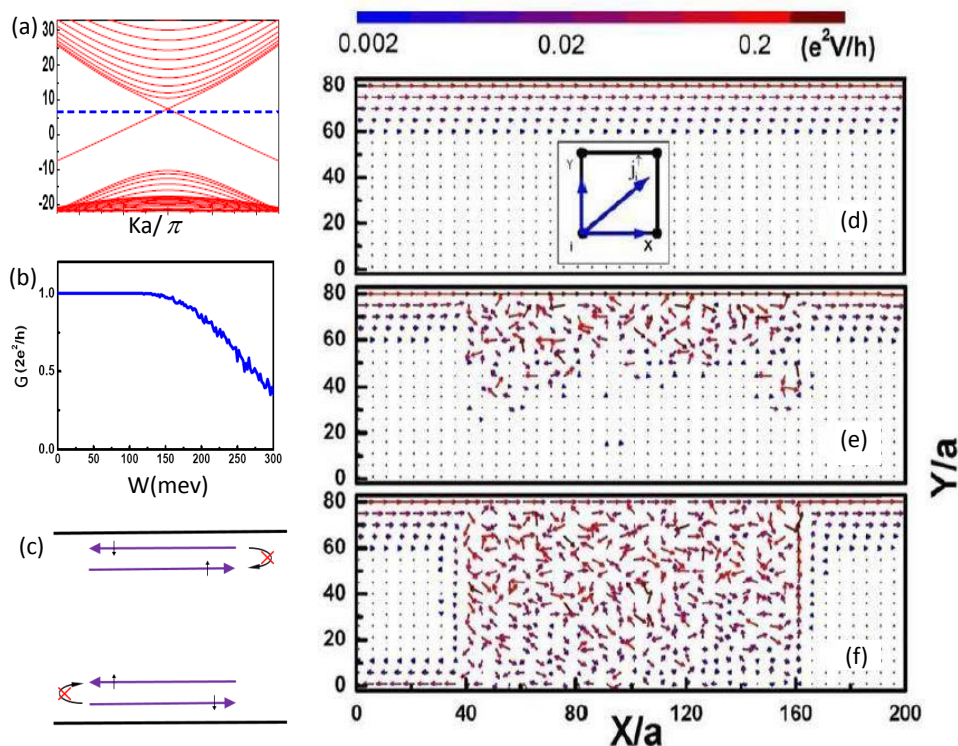


Fig. 1. (color online) (a) Typical energy spectrum for a HgTe/CdTe quantum well strip in the QSHE region. (b) The conductance G vs disorder strength W in a two terminal device. The Fermi energy is located inside the inverted gap. (c) Schematic of helical edge states propagation in the boundary of sample. On a given edge, the carriers with opposite spin polarizations propagate in opposite directions. (d) - (f) Configurations of the local current flow vector in a device with central region size $L_x = 200a, L_y = 80a$ under disorder strength (d) $W = 0$, (e) $W = 110\text{meV}$, and (f) $W = 220\text{meV}$. The inset of (d) is the schematic of local current flow vector. The direction and length of the arrows represent the local current direction and magnitude. The order of magnitude of the local currents are displayed in the color bar. Adapted from Ref.³⁰

For HgTe/CdTe quantum wells of moderate thickness, due to the strong spin-orbit coupling in this material, the system can enter a new topological phase—the QSH phase^{24,42,43}. In Fig. 1(a), the energy spectrum for the quasi one-dimensional strip is plotted. There exists an inverted bulk energy gap with two degenerate energy bands (helical edge states) that cross inside the gap. When the Fermi energy is located inside the gap, e.g. $\varepsilon_F = 7\text{meV}$, the QSH phase is established. To show how the transport properties of QSH phase are influenced by the disorder, a device with two terminals and a disordered central region is considered. Fig. 1(b) shows the two terminal conductance G versus the disorder strength W for the state shown in Fig. 1(a). For a range of disorder strength $W \in [0\text{meV}, 150\text{meV}]$, the conductance G takes the quantized value $2e^2/h$. Such an observation means that the QSHE is robust against weak disorder. Preliminarily, the behavior of the conductance G can be understood on the basis of spatial distribution of the helical edge states, as shown in Fig. 1(c). In the absence of disorder, the spin up channel on the top boundary and the spin down channel on bottom boundary give rise to the $G = 2e^2/h$. In the presence of nonmagnetic disorder, time-reversal symmetry forbids the backscattering on a given edge³⁴. Since the backscattering between the edge channels on the opposite boundaries decays exponentially due to the spatial separation, G shows a plateau with $G = 2e^2/h$ without fluctuations.

Next, in order to illustrate clearly the evolution of the conductance G versus disorder, the typical distributions of local currents in the device are plotted in Fig. 1(d)-(f). Note that only the local currents for spin-up subsystem are demonstrated. The local currents for the spin-down subsystem can be directly obtained by applying the time-reversal symmetry. In a clean sample [Fig. 1(d)], the local currents are mainly located on the upper edge and their values

decay exponentially toward the bulk. The local currents spread into the bulk and the edge channel is broadened when disorder is introduced [Fig. 1(e)]. However, not until the disorder strength W exceeds the critical value W_c , can the spreading local current connect with the bottom edge channels, which have the opposite chirality. At this point, effective backscattering [Fig. 1(f)] can occur, leading to a decrease in the conductance G between the two terminals. These pictures explain why G is robust against weak disorder and how it is destroyed in the strong disorder limit.

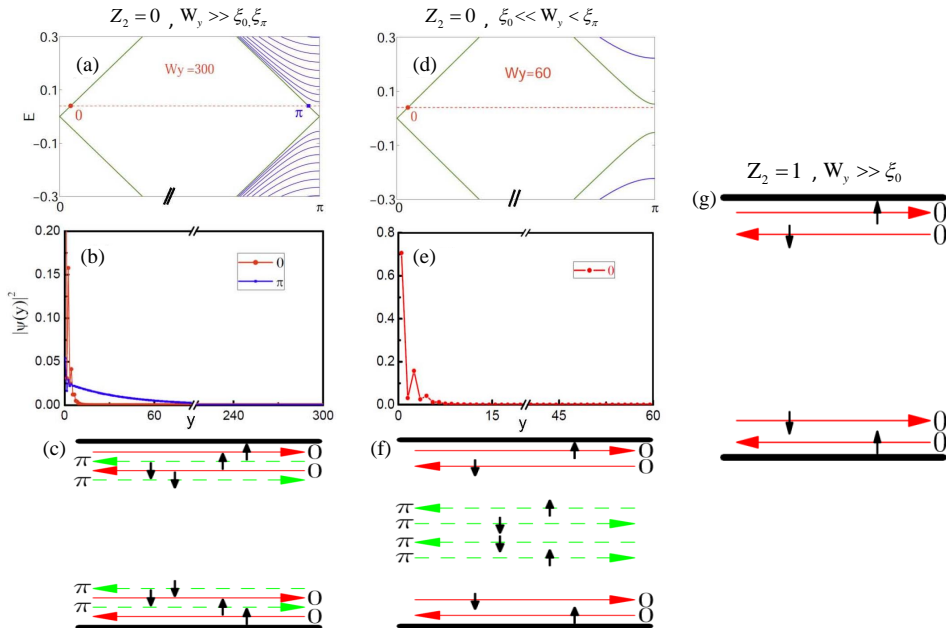


Fig. 2. (color online)(a),(d) One dimensional energy bands for the 2D anisotropic BHZ stripe with $Z_2 = 0$ and sample width $W_y = 300$ (a), 60 (d) described in the main text. (b),(e) show distribution of edge states in real space corresponding to (a) and (d) with fixed Fermi energy. (c) and (f) show schematic plots of helical edge modes corresponding to (a) and (d), respectively. The vertical arrows represent the electron spin. In panel (f), the helical edge channels around $k_x = \pi$ are hybridized due to finite size confinement, leaving one pair of helical edge channels around $k_x = 0$. Thus, these conducting channels resemble the helical edge channels in a $Z_2 = 1$ QSHE. Panels (c),(f) and (g) are adapted from Ref.³¹.

Topological insulators protected by time-reversal symmetry are characterized by the topological invariant number Z_2 ¹³. There exist odd pairs of helical surface/edge states in topological insulators with $Z_2 = 1$, which are robust and insensitive to material details and to external perturbations, as demonstrated in Fig. 1. However, most real materials with time reversal symmetry have $Z_2 = 0$ topological order, and systems with $Z_2 = 1$ topological order are very rare. Indeed, the QSHE (two-dimensional topological insulator with $Z_2 = 1$) has been experimentally confirmed only in HgTe/CdTe²⁴ and InAs/GaSb^{44,45} quantum wells. It is natural to ask, whether the $Z_2 = 1$ is a necessary requirement to realize topological surface/edge states.

According to the popular view, $Z_2 = 0$ topological systems have even pairs of helical surface/edge states, which are fragile in the presence of disorder^{40,46}. However, we find that for some $Z_2 = 0$ systems, robust transport can be engineered using a combination of finite size confinement and anisotropy³¹. With the help of the anisotropic Bernevig-Hughes-Zhang (BHZ) model^{42,43}, we demonstrate how robustness against disorder arises in such topological states.

In an anisotropic, $Z_2 = 0$ BHZ stripe, for certain parameters, there are two pairs of helical edge states around $k = 0$ and $k = \pi$ [Fig. 2(a)]. The 0 helical edge states are located close to the edge, while the π helical edge states are more delocalized toward the bulk [Fig. 2(b)]. When the stripe is sufficiently wide, [i.e. $W_y = 300$, which is much greater than the decay length of both the 0 and π helical edge channels], both $k = 0$ and π helical edge bands are

nearly gapless as expected. As a consequence, the Fermi energy crosses the $k = 0$ helical edge states and counter-propagating π edge states, which also have substantial real-space overlap [Fig. 2(c)]. The disorder can heavily couple these two states and cause strong backscattering between the $k = 0$ and $k = \pi$ edge channels, leading to complete localization. In transport experiments, such a stripe then resembles a normal insulator. In contrast, when the stripe becomes narrow [i.e. $W_y = 60$], the 0 helical edge bands remain almost gapless, while the coupling of extended π helical edge states opens a remarkable hybridization gap Δ [Fig. 2(d)]. When the Fermi energy is located inside the gap Δ , only the $k = 0$ helical edge states exist. Therefore, the $k = 0$ helical edge states are well separated with the $k = \pi$ states. In addition, since the decay length of 0 helical edge states, ξ_0 , is much shorter than the sample width W_y , the $k = 0$ helical edge states on the top edge are also well separated with that on the bottom edge [Fig. 2(e) and (f)]. From a transport point of view, the conducting edge channels in Fig. 2(f) [$Z_2 = 0$] are similar to those in Fig. 2(g) and Fig. 1(c) [$Z_2 = 1$]. Conclusively, then despite having a topological number $Z_2 = 0$, the helical edge states in Fig. 2(f) emerge as being robust.

In order to quantitatively assess the robustness of these emerging $Z_2 = 0$ helical edge states, their transport properties under nonmagnetic disorder in a two terminal device and a π -bar device [Fig. 3(a) and 3(e)] are simulated. The results are demonstrated in Fig. 3(c) and 3(e), respectively. For comparison, the transport properties of these two devices incorporating (i) normal $Z_2 = 0$ states with two pairs of helical edge states [Fig. 3(b) and 3(f)] and (ii) $Z_2 = 1$ QSHE [Fig. 3(d) and 3(h)] are also obtained. In the case of emergent helical edge states, the two terminal conductance $G_{12,12}$ shows a quantized plateau $2e^2/h$ in the clean limit. When nonmagnetic disorder is introduced, the $2e^2/h$ plateau remains unchanged without fluctuation [Fig. 3(c)]. Meanwhile, the nonlocal conductance $G_{14,23}$ in the π -bar device shows well quantized plateaus at $4e^2/h$, irrespective of details of the terminals and the strength of the strong disorder [Fig. 3(g)]. Therefore, the transport properties of the emergent helical states are completely different from normal $Z_2 = 0$ states cases, where $G_{12,12}$ and $G_{14,23}$ are found that are fragile against disorder. Instead, the $G_{12,12}$ and $G_{14,23}$ cases behave exactly like a $Z_2 = 1$ QSHE system, see Figs. 3(d) and 3(h), and the experimental results in⁴⁵. The two-terminal perfect $2e^2/h$ plateau and the π -bar perfect $4e^2/h$ plateau plausibly provide a transport definition of robust helical edge states in these $Z_2 = 0$ systems. In a $Z_2 = 1$ QSHE, the robustness of the edge conduction is derived from its intrinsic topological character. On the other hand, the robust helical edge states in the $Z_2 = 0$ model arise from the fact that the backscattering is detuned by the finite size confinement.

Besides the anisotropic BHZ model, the $Z_2 = 0$ topological systems involving helical surface states with emergent robustness have been extended into several 2D and 3D models^{31,47-49}. In addition, two systems built on realistic materials: (i) Dirac semi-metal with appropriate width and thickness confinement⁵⁰ and (ii) a bismuth (111) film with a thickness of between 20 and 70 nm^{31,51} are proposed to host robust helical surface states. Recent relevant experiments have shown the clues of the existence of such topological states in the latter proposed material system^{51,52}. It is worth noting that the proposed $Z_2 = 0$ systems have additional exotic properties not present in $Z_2 = 1$ QSHE, which can be utilized to fabricate new topological devices⁵⁰.

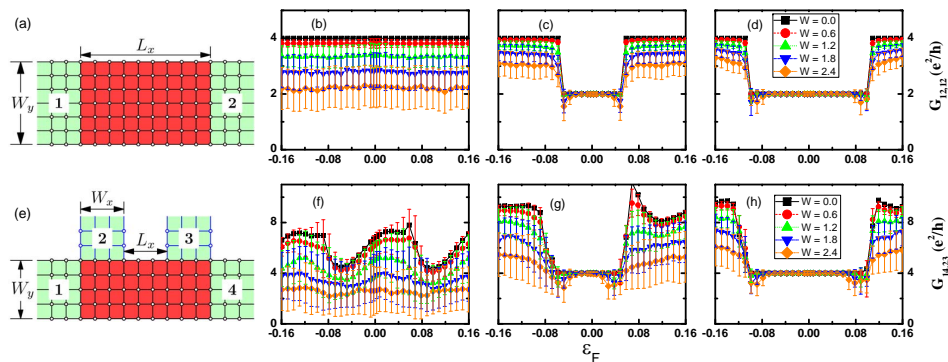


Fig. 3. (color online) (a), (e) Illustration of two-terminal and π -bar devices. The Anderson disorder exists only in the central (red) region. The size parameters are $L_x = 120$, $W_x = 120$, $W_y = 60$. (b) (d) Two-terminal conductance $G_{12,12}$ of device (a); (f) (h) nonlocal conductance $G_{14,23}$ of device (e) vs the Fermi energy ε_F for different disorder strengths W for the cases of a normal $Z_2 = 0$ system (b) and (f); $Z_2 = 0$ topological system with emergent robust helical edge states (c) and (g) and $Z_2 = 1$ QSHE (d) and (h). $G_{14,23}$ means that the current I_{14} is injected from terminal 1 to 4 and the voltage V_{23} is measured between terminal 2 and 3 and $G_{14,23} = \frac{V_{23}}{I_{14}}$. The error bars denote the conductance fluctuation. Adapted from ref.³¹

III. DISORDER INDUCED TOPOLOGICAL INSULATORS

Besides destroying topological states, in special systems, moderate disorder can also produce topological states. The first well studied disorder induced topological state was the topological Anderson insulator (TAI). Specifically, in the clean limit, the system is in an ordinary insulator or metal. With the introduction of disorder, it enters into a topological insulator state with robust transport. This TAI was predicted to arise in HgTe/CdTe quantum wells by Shen's group⁵³ and our group³⁰. This type of TAI was then extended to many other systems^{54–65}.

Let us begin with a review of how TAI arises in HgTe/CdTe quantum wells. In the clean limit, the system is described by the BHZ model⁴²

$$\begin{aligned} \mathcal{H}_l(\vec{k}) &= \begin{pmatrix} h_0(\vec{k}) & 0 \\ 0 & h_0^*(-\vec{k}) \end{pmatrix}, \\ h_0(\vec{k}) &= \varepsilon(\vec{k}) + d_\alpha(\vec{k})\sigma_\alpha, \end{aligned} \quad (1)$$

where σ_α [$\alpha = x, y, z$] are the Pauli matrices, and

$$\begin{aligned} \varepsilon(\vec{k}) &= C - D(k_x^2 + k_y^2), \\ \mathbf{d}(\vec{k}) &= [Ak_x, Ak_y, M - B(k_x^2 + k_y^2)]. \end{aligned} \quad (2)$$

A, B, C, D, M are material parameters. Specially, M is the topological mass, which can be tuned continuously through the thickness of the HgTe layer. If $M < 0$, the bulk band is inverted and the system becomes to a QSHE [Fig. 4(b)]. In contrast, if $M > 0$, the system becomes a normal insulator [Fig. 4(e)].

In Fig. 4(a) and 4(d), which is taken from Ref⁵³ Li et al plot the two terminal conductance G versus the disorder strength W for different Fermi energies ε_F . When the Fermi energy ε_F is in the valence band, then for both $M < 0$ and $M > 0$, G quickly decreases to zero as the disorder strength W increases [green line in 4(a) and 4(d)]. In sharp contrast, if ε_F is located near the edge of the conduction band, for both $M < 0$ and $M > 0$ G first decreases when Anderson disorder is introduced. Intriguingly, continuously increasing the disorder strength W does not lead to the localization of the system, but makes G increase again up to a quantized value. This value is maintained for a certain

range without fluctuations [blue line in 4(a) and 4(d)]. As described in section II, the $2e^2/h$ plateau signals that the system has entered a new topological state, referred above as the TAI. Further, the nature of the TAI is clarified by the phase diagrams shown in Fig. 4(c) [$M < 0$] and in Fig. 4(f) [$M > 0$]. Significantly, for $M > 0$, there are no topological helical edge states in the clean limit [Fig. 4(e)]. The quantized plateau cannot be attributed to the coexistence of the bulk and edge states, and the disorder causes the localization of the bulk states. It therefore seems that Anderson disorder creates the helical edge state, and leads to robust transport.

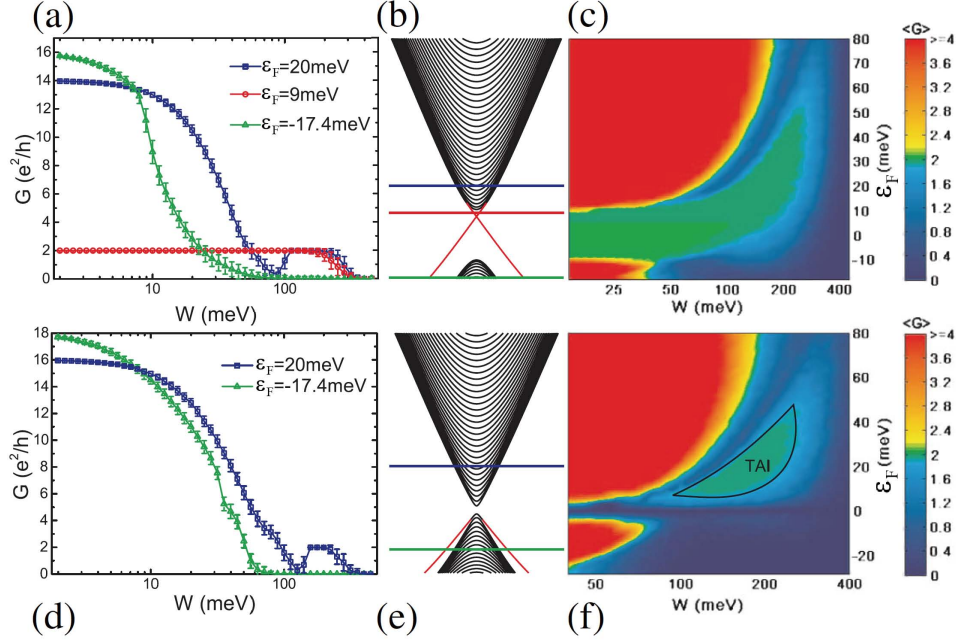


Fig. 4. (color online) Conductance of disordered strips of HgTe/CdTe quantum wells. (a)-(c) and (d)-(f) show results for an inverted quantum well with $M = -10\text{meV}$ and for a normal quantum well with $M = 1\text{meV}$, respectively. (a) The conductance G versus disorder strength W at three values of Fermi energy. The error bars represent the conductance fluctuations. (b) One dimensional energy spectrum. The vertical scale (energy) is the same as in (c) and the horizontal lines correspond to the values of the Fermi energy considered in (a). (c) Phase diagram showing the conductance G as a function of both disorder strength W and Fermi energy ε_F . The panels (d), (e), and (f) are the same as (a), (b), and (c), but for $M > 0$. The TAI phase is shown in green region. In all panels, the strip width is 500nm and the length is 5000nm in (a) and (d), and 2000nm in (c) and (f). Adapted from Ref.⁵³.

To validate this assumption, we study the evolution of the local current configurations under different disorder strengths [Fig. 5]³⁰. The parameters were set to be $M = 2\text{meV}$ and $\varepsilon_F = 18\text{meV}$ [Fig. (5a)]. The plot of G vs W in Fig. 5(b) can be subdivided into four regions (i) without disorder, (ii) before the anomalous plateau, (iii) on the anomalous plateau, and (iv) after the anomalous plateau. Typical spatial distributions of the local currents are plotted in Fig. 5(h)-(k), respectively. The most interesting phenomena are to be found in region (iii) [Fig. 5(i)]. Here, the local currents in the bulk decline to zero while the residual currents flow around the upper edge with little scattering [only the spin up subsystem is considered]. In addition, throughout region (iii), the bulk transport vanishes and the edge transport shows the same behavior as in the traditional QSHE region [Fig. 1(d)-(f)]. The local currents shown in Fig. 5 provides strong evidence that disorder leads to the helical edge states and hence to the TAI.

Based on the discoveries described in references^{30,53}, Groth et al. present an effective medium theory that explains the physical origin of the TAI⁶⁶. Disorder can induce a self-energy Σ . In the self-consistent Born approximation (SCBA), Σ is given by⁶⁷:

$$\Sigma = \frac{W^2}{12} (a/2\pi)^2 \int_{\text{BZ}} d\vec{k} \left[\sigma_\alpha \left(\varepsilon_F^\pm - h_0(\vec{k}) - \Sigma \right)^{-1} \sigma_\alpha \right]. \quad (3)$$

Here σ_α denotes the type of disorder, and a is the lattice constant. Σ can be decomposed into the form $\Sigma = \Sigma_0\sigma_0 + \Sigma_x\sigma_x + \Sigma_y\sigma_y + \Sigma_z\sigma_z$. Therefore, the self energy, Σ , makes a correction to the original Hamiltonian $h_0(\vec{k})$ and renormalizes the topological mass and the Fermi energy:

$$\bar{M} = M + \text{Re}\Sigma_z, \quad \bar{\varepsilon}_F = \varepsilon_F + \text{Re}\Sigma_0. \quad (4)$$

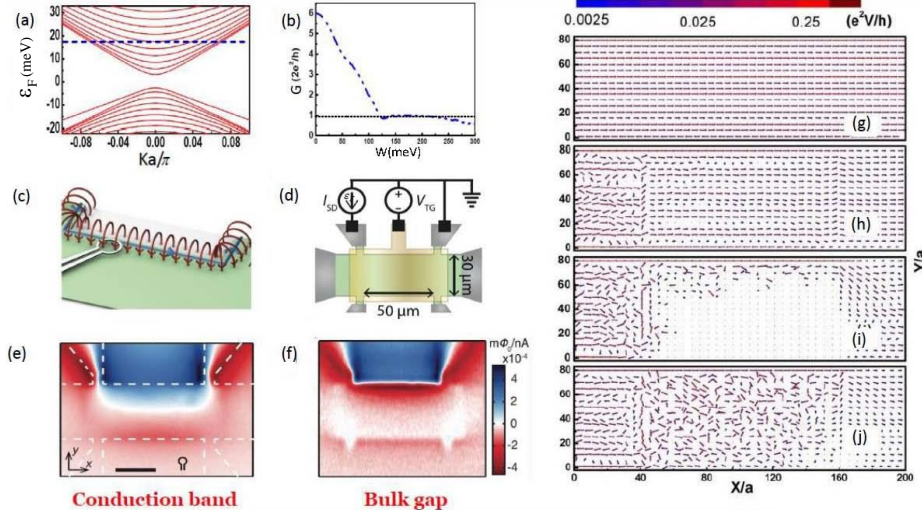


Fig. 5. (color online) (a) Typical one-dimensional energy spectrum for a normal HgTe/CdTe quantum well strip. (b) Conductance G vs disorder strength W . (g)-(j) Configurations of the local current flow vector for the strip with the same sample sizes as for Fig. 1, and with the disorder strength set at (g) $W = 0$, (h) $W = 100 \text{ meV}$, (i) $W = 150 \text{ meV}$, and (j) $W = 250 \text{ meV}$. In (a),(b),(g)-(j), The Fermi energy and topological mass are set to be $\varepsilon_F = 18 \text{ meV}$ and $M = 2 \text{ meV}$. (c) Sketch of the configurations for the local current flow measurement. The magnetic field (red) generated by the current (blue) is measured by detecting the flux through the SQUID's pickup loop. (d) Schematic of a Hall bar. (e)(f) Typical measured distributions of the local current when Fermi energy is inside the conduction band (e) and the bulk gap (f), respectively. (a)(b)(g)-(j) are reproduced from Ref.³⁰. (c)-(f) are adapted from Ref.¹⁰⁸.

Groth et al⁶⁶ found that the Anderson type of disorder $[\sigma_{0,z}]$ can make a negative correction $[\text{Re}\Sigma_z < 0]$ to the topological mass M . Thus, it can lead a transition of \bar{M} from positive to negative by increasing the disorder strength. Moreover, due to lacking the particle-hole symmetry of $h_0(\vec{k})$, the Anderson disorder also makes a negative correction to the Fermi energy ε_F . When ε_F is in the conduction band, for both $M > 0$ and $M < 0$, the Anderson disorder can tune the renormalized Fermi energy $\bar{\varepsilon}_F$ into the inverted gap $[-|\bar{M}|, |\bar{M}|]$. The TAI phase is then established. In contrast, when ε_F is in the valence band, $\bar{\varepsilon}_F$ is shifted away from the gap. G quickly decays to zero and no quantized conductance appears.

If the effective medium theory is correct, one can deduce from Eq.(3) that the emergence of TAI is highly relevant to the type of disorder. Concretely, the σ_z term exists in $(\varepsilon_F^+ - h_0(\vec{k}) - \Sigma)^{-1}$. While Anderson disorder ($\sigma_{0,z}$) makes a negative correction ($\sigma_0\sigma_z\sigma_0 = \sigma_z\sigma_z\sigma_z = \sigma_z$) to the topological mass M , the bond disorder ($\sigma_{x,y}$) results in a positive correction ($\sigma_x\sigma_z\sigma_x = \sigma_y\sigma_z\sigma_y = -\sigma_z$) to M . To see this more clearly, in Fig. 6, we compare the conductance phase diagrams for Anderson disorder and bond disorder in the HgTe/CdTe quantum wells with $M = 1 \text{ meV}$ ⁶⁸. It can be seen from Fig. 6(a), that at moderate Anderson disorder and with an appropriate Fermi energy, a clear TAI phase [green region] is present, and such a TAI phase should correspond to a negative renormalized topological mass \bar{M} [blue region in Fig. 6(c)]. When referring to the bond disorder case, for any disorder strength W and Fermi energy ε_F , \bar{M} is always positive. Correspondingly, there is no indication of the TAI phenomenon in Fig. 6(b). From Fig. 6, one can conclude that normal Anderson disorder gives rise to the TAI phenomenon and bond disorder destroys it.

The results not only verify the validity of the effective medium theory, but also are important for the experimental realization of the TAI phase.

To date, the physical properties of the TAI phase have been extensively studied^{69–75}, and several significant advances are worth noting. In Fig. 4(f) and Fig. 6(a), since it is surrounded by a normal Anderson insulator phase, the TAI phase was initially considered to be a new topological phase. Later, using a three dimensional phase diagram [disorder strength W , Fermi energy ε_F and topological mass M], Prodan found that the TAI phase is not a distinct phase but part of the quantum spin-Hall phase, because these two phases can be adiabatically connected by varying the topological mass⁶⁹. Xu et al studied the phenomenon in a very large sample, and a complete phase diagram of the TAI phase was obtained⁷⁰. They found that the TAI phase region was much larger than what SCBA theory predicted. The reason is that the TAI can exist in a mobility gap rather than an inverted band gap^{70,71}.

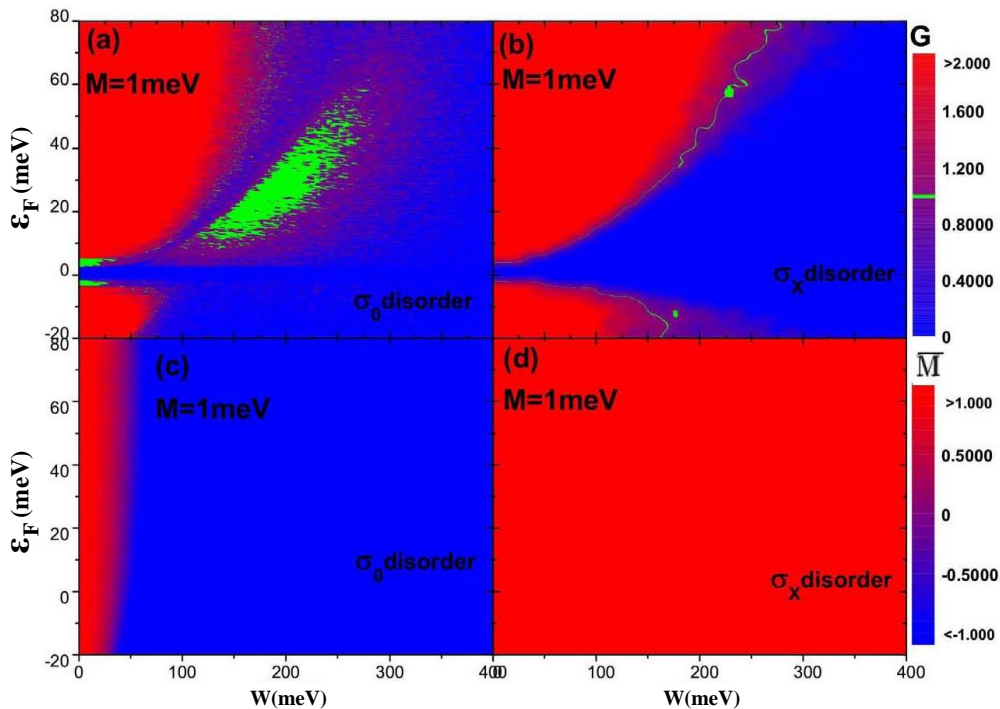


Fig. 6. (color online) The conductance G (a), (b) and renormalized topological mass \bar{M} (c), (d) vs disorder strength W and Fermi energy ε_F for the HgTe/CdTe model with $M = 1\text{meV}$. Here, σ_0 and σ_x correspond to Anderson disorder and bond disorder, respectively. Adapted from Ref.⁶⁸

In what follows, we introduce another type of topological state induced by disorder. Compared to the above TAI state, there are several differences. First, such a state is not triggered by the disorder strength but the randomness of the adatom configuration. Second, such a state cannot be explained by the effective medium theory. Third and of the greatest importance, contrary to the common view, such disorder induced topological states are much easier to be realized than the normal insulator state in the periodic case.

Because of the outstanding properties of its electronic structure, graphene is considered as an ideal platform to host topological phases. For instance, recent first-principles calculations proposed that certain nonmagnetic adatoms (e.g., indium and thallium) could enhance the intrinsic spin-orbit coupling to give rise to the QSHE^{76–78}; and some magnetic adatoms (e.g., 3d and 5d transition metals) could induce sizable Rashba spin-orbit coupling and magnetization to produce the quantized anomalous Hall effect (QAHE)^{79–81}. Though great theoretical progress has been achieved, no experimental observation has been reported. There are two major reasons preventing the experimental exploration of

these novel states. (i) All the calculations are based on the periodic adsorption condition, which is beyond existing experimental capabilities. (ii) The formation of topological states is highly dependent on the adatom configurations. At certain coverage rates, the system is a trivial insulator.

Let us first explain why the topological nontrivial state and trivial insulator state can exist in the periodic adsorption case with different coverage rates. As illustrated in Fig. 7(a) and (b), the tight-binding Hamiltonian of graphene with non-magnetic adatoms can be written as^{32,82}:

$$\begin{aligned} H &= H_0 + H_{\text{so}} + H_U \\ &= -t \sum_{\langle ij \rangle, \alpha} c_{i\alpha}^\dagger c_{j\alpha} + i\lambda_{\text{SO}} \sum_{\langle\langle ij \rangle\rangle \in \mathcal{R}, \alpha\beta} \nu_{ij} c_{i\alpha}^\dagger s_{\alpha\beta}^z c_{j\beta} + U \sum_{i \in \mathcal{R}, \alpha} c_{i\alpha}^\dagger c_{i\alpha}. \end{aligned} \quad (5)$$

The presence of the adatom at \mathcal{R} not only enhances the intrinsic SOC term (H_{so}) but also generates the on site potential term (H_U) with respect to \mathcal{R} to the surrounding carbon atoms. H_{so} induces a topologically nontrivial gap Δ_{so} at both K and K' with magnitude

$$\begin{aligned} \Delta_{\text{so}} &\propto \sum_{\mathcal{R}} H_{\text{so}}(\mathcal{R}) e^{i(K-K') \cdot \mathcal{R}} = \sum_{\mathcal{R}} H_{\text{so}}(\mathcal{R}) e^{i(K'-K') \cdot \mathcal{R}} \\ &= \sum_{\mathcal{R}} H_{\text{so}}(\mathcal{R}) \end{aligned} \quad (6)$$

and H_U induces the inter-valley scattering, which results in a topological trivial gap Δ_U with magnitude

$$\Delta_U \propto \sum_{\mathcal{R}} H_U(\mathcal{R}) e^{i(K-K') \cdot \mathcal{R}}. \quad (7)$$

When adatoms form a $\sqrt{3}n \times \sqrt{3}n$ or $3n \times 3n$ supercell, a finite Δ_U can be obtained since the factor $e^{i(K-K') \cdot \mathcal{R}} = 1$ for all \mathcal{R} . Because the on-site potential U is much larger than the intrinsic SOC λ_{so} , the topological trivial gap Δ_U exceeds the topological nontrivial gap Δ_{so} , resulting in a trivial insulator state. For other periodic adsorption cases, the inequivalent $e^{i(K-K') \cdot \mathcal{R}}$ for various \mathcal{R} vanishes the inter-valley scattering [$\Delta_U \rightarrow 0$]. Since $\Delta_{\text{so}} > \Delta_U$, a quantum spin Hall state is realized³².

Interestingly, when the adatoms are nonuniformly distributed in space, the factor $e^{i(K-K') \cdot \mathcal{R}}$ becomes randomized. As a result, even when adatom is at the coverage rate $\frac{1}{3n^2}$ or $\frac{1}{9n^2}$, such randomization reduces Δ_U from a large value in periodical case to nearly zero in the random adsorption case. We note the renormalization process for Δ_U cannot be described by the effective medium case. In sharp contrast, the topologically nontrivial gap Δ_{so} is caused by zero momentum scattering. From Eq. (6), the randomization of the adatom distribution plays a negligible role in determining the magnitude of Δ_{so} . Therefore, one can expect a quantum phase transition from trivial insulator state [$\Delta_{\text{so}} < \Delta_U$] to a topological insulator state [$\Delta_{\text{so}} > \Delta_U$] with the introduction of the spatial randomness of the adsorbates.

As an example, we study the possibility of realizing QSHE states in graphene with randomly distributed adsorbates. Fig. 7(c) shows the results of a simulation of the transport properties of the system with a 11.1% coverage ratio [3×3 supercell]. For the case of periodically distributed adatoms [Fig. 7(a)], a zero two terminal conductance $G = 0$ is observed in the region where $\varepsilon_F \in [0.117t, 0.124t]$, signaling a trivial insulator. However, when the adatoms become randomly distributed [Fig. 7(b)], a quantized plateau $G = 2e^2/h$ with vanishing fluctuation emerges within the range $\varepsilon_F \in [0.116t, 0.132t]$, indicating that the system turns into the quantum spin Hall phase. Fig. 7(d) shows a simulation

of the transport properties of the system with a 6.25% coverage ratio [4×4 supercell]. The robust quantized plateau $G = 2e^2/h$ for both two cases shows that the topological phase predicted from first-principles is not affected by the randomization of the adatom configurations. In Fig. 7(e), we show that randomization of magnetic adatoms can also turn graphene from a trivial insulator to a QAHE^{32,82}.

The above adatom adsorption studies suggest that in a realistic graphene sample, the topological state is the favored ground state. Therefore, this calculation provides evidence of the high possibility of realizing topological phases in graphene³².

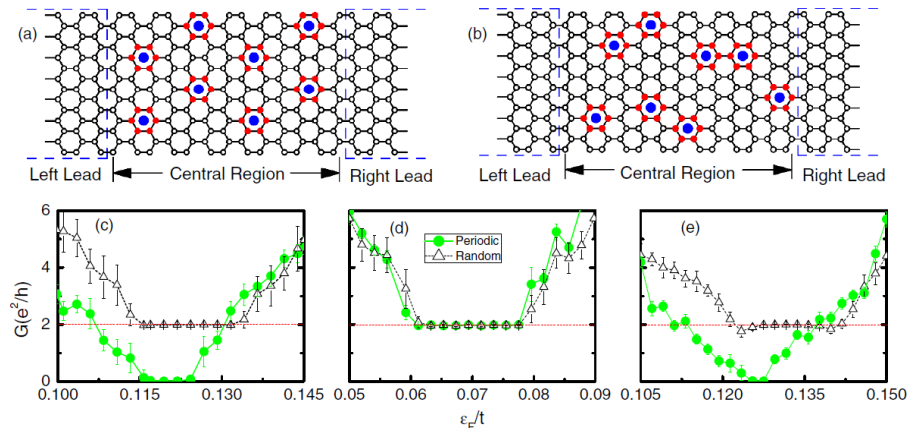


Fig. 7. (color online)(a)(b) Schematic of a two-terminal device with periodically and randomly distributed adatoms, respectively. Both adatom coverages are 11.1%.(c)(e) Comparison of conductances G between periodic and random adsorption as a function of Fermi level ε_F . (c)(d) The site potential and intrinsic SOC are set to $U = 0.36t$ and $\lambda_{SO} = 0.016t$. The adatom coverages are 11.1% in panel (c) and 6.25% in panel (d). In (e) the adatom coverage is 11.1%. Circle and triangle symbols represent the periodic and random adatoms. The error bars denote the conductance fluctuations. Adapted from Ref.³⁰

IV. METAL-INSULATOR TRANSITION

Since it was first proposed by P. W. Anderson, the disorder induced metal-insulator transition has been a long lasting, interesting research issue in condensed matter physics⁸³. According to scaling theory, the metal-insulator transition in a material system depends on its universality ensemble [symplectic, unitary and orthogonal] and dimension^{84–86}. Initially, it was believed that the extended states (metal) could exist only in three-dimensional systems and that all the bulk states in two and one-dimensional systems were localized (insulator)⁸⁴. Later, two exceptions were found in two-dimensional systems. One was a the system with strong spin-orbital coupling [symplectic ensemble]. The other was a system without time reversal symmetry [unitary ensemble]. The topological states always share these two features and then become the focus of research on the metal-insulator transition. In the past two decades, the metal-insulator transition in quantum Hall systems has been clearly understood^{87–89}. The extended state can only exist at the transition point between different plateaus. The critical exponents of the transition have also been obtained. In the last few years, there have been many studies of the metal-insulator transition in a QSHE^{90–94}. Their results can be summarized as follows (i for a QSHE with Rashba spin-orbital coupling, the system belongs to a symplectic ensemble. A metallic phase emerges between the QSH phase and the normal insulator phase; (ii) for a QSHE without Rashba spin-orbital coupling, the system can be divided into two spin subsystems, both of which belong to unitary ensemble. A direct transition from a QSHE to a normal insulator is observed. Though the metal-insulator transition in two-dimensional topological states has been extensively studied, the transition properties in three-dimensional

topological states are still not quite clear.

More recently, the Weyl semimetal (WSM), a gapless topological state in three-dimension, has been theoretically predicted and experimentally confirmed^{18,19,21}. Thus, it is timely to study the effects of disorder and metal-insulator transition both for their direct experimental relevance and for their fundamental value in advancing the understanding of the interplay between randomness and topological order. In reference³³, we do so by using both numerical and analytical approaches. Different from the previous studies that only concentrate on single weyl node⁹⁵⁻⁹⁷, we focus on a more realistic tight-binding model with considering the interplay of opposite weyl nodes^{98,99}. By calculating the localization length¹⁰⁰ and the Hall conductivity^{101,102}, we obtain the complete phase of the system under all the disorder strength. Because the WSM has novel gapless excitations, i.e. the Weyl nodes in the bulk and Fermi arcs on the surface, we find an unexpected rich phase diagram, as shown in Fig. 8(c). With increasing disorder strength, the system undergoes multiple phase transitions. For example, one can obtain (i) 3D quantum anomalous Hall state (QAH) -3D diffusive anomalous Hall metal (metal) - normal insulator (NI); (ii) WSM - QAH-metal-NI ; (iii) WSM-metal-NI; (iv) NI-WSM-metal-NI in Fig. 8(a),(b),(d),(e) respectively. Through the comprehensive study of the phase diagram, we first address the important issue on the stability of the Weyl nodes and Fermi arcs against weak disorder. The weak disorder has important effects when the Weyl nodes are close in momentum space. The WSM to QAH and the NI to WSM transitions are caused by the pair annihilation near the zone boundary and pair nucleation at the zone center. Then, we find the the transition from WSM to metal by moderate disorder is unconventional. This transition takes place between two metallic states and is only enabled by the topological character of the Weyl nodes.

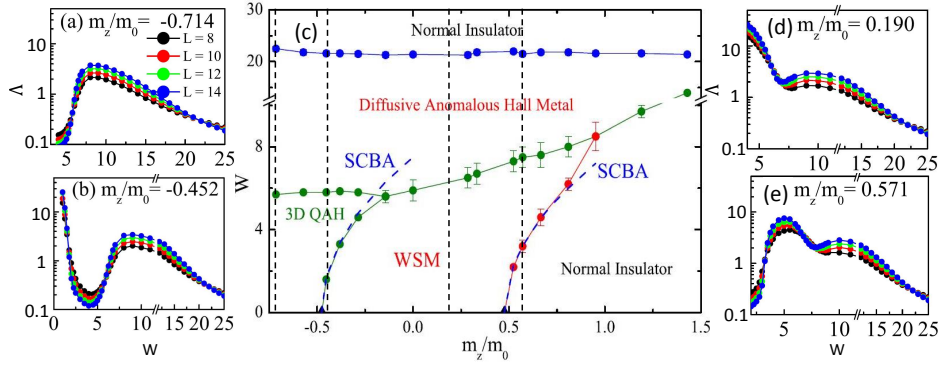


Fig. 8. (color online) (a),(b),(d),(e) Normalized localization length $\Lambda = \lambda(L)/L$ vs disorder strength W for different masses m_z [lines in subplot (c)]. $\lambda(L)$ is the localization length of a long bar sample with cross section $L \times L$. An increase in Λ with L signals a metal phase, while a decrease with L signals an insulator phase. When Λ is independent of L , this signals a critical point of the phase transition. (c) Phase diagram in the $W - m_z$ plane. The symbols guided by the solid lines were obtained from the normalized localization length. The dashed blue lines are the phase boundaries determined using the SCBA. In a finite layer sample, the 3D QAH, WSM and Diffusive anomalous Hall metal phases are distinguished by its Hall conductance being quantized and equivalent to to layer number, being quantized, and being non-quantized, respectively. Adapted from³³

It is worth noting that independent of our work, Liu et al also studied the disorder induced metal-insulator transition in 3D QAH layer systems and observed a rich phase diagram¹⁰³. Moreover, the unconventional WSM to metal transition has also generate broad interest, and the critical exponent of the transition has been obtained¹⁰³⁻¹⁰⁵.

V. CONCLUSIONS AND OUTLOOK

In this paper, based on reviewing our own disorder studies and other relevant works produced over the last few years, recent developments into the effects of disorder in topological states are briefly summarized. We show that all of weak, moderate and strong disorder can lead to exotic phenomena in various type of topological states. How these phenomena originate from the topologically nontrivial nature of topological states is also demonstrated. In spite of significant recent progress, there is nevertheless still plenty of room for further research into the effects of disorder in topological states. Before concluding the review, we discuss the opportunities for disorder studies in the future.

Experimental and material realization of disorder related topological phases. Seven years after its first prediction^{30,53}, the first signs of the experimental realization of the TAI phase have now been found. However, the host system is evanescently coupled waveguides^{55,106}. Due to the recent great advance in controlling the disorder strength¹⁰⁷ and in the measurement of the local current¹⁰⁸ in topological material, we expect the TAI phase can soon be confirmed in condensed matter systems. It is also to be noted that the topological phase in graphene has promising applications in information processing. We have demonstrated that both QSHE and QAHE states in graphene can easily be engineered through randomly adsorbing nonmagnetic/magnetic adatoms³². We also expect the experimental observation of these topological states.

Understanding the fundamental phenomena caused by the disorder. By now, our understanding of many disorder related phenomena is still limited. Firstly, it is a common belief that 2D unitary system is scaled to insulator except at some isolated critical points⁸⁶. However, in reference¹⁰⁹ and reference¹¹⁰, though the considered models are totally different, we find in both a novel metallic phase region that may emerge between QSHE and normal insulator phases. The physical origins for the metallic phase and the relationship between these two models should also be carefully addressed. Secondly, analogue to disorder induced Anderson localization benefits the observation of quantized Hall plateaus in QHE, the disorder also plays an important role in the experimental observation of the QSHE and QAHE^{44,45}. Du et al find that dilute silicon impurity doping in InAs/GaSb quantum wells can greatly suppress residual bulk conductance and produce a perfect QSHE⁴⁵. From the point of view of theory, despite the attempt to study the phenomena⁵⁷, the mechanism for the effects of impurity doping on the transport properties of the system is still not clear. Significantly, there exist great puzzles regarding disorder effects in thin films of chromium-doped $(\text{Bi,Sb})_2\text{Te}_3$, which is key to understand why the QAHE can only be observed at extremely low temperatures^{11,111}. Thirdly, type-II Weyl semimetals, which harbor unconventional Weyl nodes, have been proposed recently¹¹². It would be interesting to study the stability of these Weyl nodes under strong disorder. Finally, dephasing effects also exist in realistic samples. A natural topic is how the transport properties of topological states are affected when both disorder and dephasing effects are considered¹¹³.

Acknowledgments: We are grateful to X. C. Xie, Q. Niu, Z. Q. Wang, Q.-F. Sun, J. R. Shi, H. W. Liu, Z. H. Qiao, J. Feng, L. Wang, Z. B. Wang, D. W. Xu and C. Z. Chen for collaboration and for their important contributions reviewed in this paper. H. J. also appreciates the discussions with J. Liu, J. H. Gao, Y. G. Yao and S. Q. Shen. This Project supported by the National Natural Science Foundation of China (Grant No.11374219, No. 11474085 and No.

11534001)

* jianghuaphy@suda.edu.cn

- ¹ Prange R E and Girvin S M 1987 *The Quantum Hall Effect*, New York, Springer
- ² Hasan M Z, and Kane C L, 2010 *Rev. Mod. Phys.* **82** 3045
- ³ Qi X L and Zhang S C, 2011 *Rev. Mod. Phys.* **83** 1057
- ⁴ Shen S Q 2012 *Topological Insulator*, Springer
- ⁵ Weng H M, Yu R, Hu X, Dai X, and Fang Z, 2015 *Adv. Phys.* **64** 227.
- ⁶ Ren Y F, Qiao Z H, Niu Q, 2015 *arXiv: 1509.09016*
- ⁷ Chiu C K, Teo J C Y, Schnyder A P, and Ryu S, 2016 *arxiv: 1505.03535*
- ⁸ Weng H M, Dai X, and Fang Z 2016 *arxiv: 1603.04744*
- ⁹ Klizing K v, Dorda G, and Pepper M, 1980 *Phys. Rev. Lett.*, **45** 494
- ¹⁰ Haldane F D M, 1988 *Phys. Rev. Lett.* **61** 2015
- ¹¹ Chang C Z, Zhang J S, Feng X, et al., 2013 *Science* **340** 167
- ¹² Kane C L and Mele E J, 2005 *Phys. Rev. Lett* **95** 226801
- ¹³ Kane C L and Mele E J, 2005 *Phys. Rev. Lett* **95** 146802
- ¹⁴ Fu L, Kane C L, and Mele E J 2007 *Phys. Rev. Lett* **98** 106803
- ¹⁵ Moore J E and Balents L 2007 *Phys. Rev. B* **75** 121306(R)
- ¹⁶ Fu L, 2011 *Phys. Rev. Lett* **106** 106802
- ¹⁷ Volovik G E 2002 *JETP. Lett* **75** 55
- ¹⁸ Wan X, Turner A M, Vishwanath A V and Savrasov S Y, 2011 *Phys. Rev. B*, **83** 205101
- ¹⁹ Lv B Q et al., 2015 *Phys. Rev. x* **5** 031013; Xu S Y et al., 2015 *Science* **349** 613
- ²⁰ Liu Z K, et al., 2014 *Science* **343**, 864
- ²¹ Weng H, Fang C, Fang Z, Bernevig B A, and X Dai, 2015 *Phys. Rev. X*, **5** 011029
- ²² Wang Z, Sun Y, Chen X Q, Franchini C, Xu G, Weng H, Dai X, and Fang Z, 2012 *Phys. Rev. B* **85**, 195320; Wang Z, Weng H, Wu Q, Dai X, and Fang Z, 2013 *Phys. Rev. B* **88** 125427.
- ²³ Thouless D J, Kohomoto M, Nightingale M P, and Nijs M D, 1982 *Phys. Rev. Lett* **49** 405
- ²⁴ König M, Wiedmann S, Bruene C, Roth A, Buhmann H, Molenkamp L W, Qi X L and Zhang S C, 2007 *Science* **318** 766
- ²⁵ Zhang T, Cheng P, et al., 2009 *Phys. Rev. Lett.* **103** 266803
- ²⁶ Chen J et al., 2010 *Phys. Rev. Lett*, **105**, 176602
- ²⁷ Lu H Z, Shi J R, and Shen S Q, 2011 *Phys. Rev. Lett.* **107** 076801
- ²⁸ Aji V 2012 *Phys. Rev. B* **85** 241101(R)
- ²⁹ Xiong J, et al., 2015 *Science* **350** 413
- ³⁰ Jiang H, Wang L, Sun Q F and Xie X C, 2009 *Phys. Rev. B* **80** 165316
- ³¹ Jiang H, Liu H W, Feng J, Sun Q F, and Xie X C, 2014 *Phys. Rev. Lett* **112** 176601
- ³² Jiang H, Qiao Z H, Liu H W, Shi J R and Qian N, 2012 *Phys. Rev. Lett* **109** 116803
- ³³ Chen C Z, Song J T, Jiang H, Sun Q F, Wang Z Q, and Xie X C, 2015 *Phys. Rev. Lett* **115** 246603
- ³⁴ Xu C K and Moore J E, 2006 *Phys. Rev. B*, **73** 045322
- ³⁵ For a brief review, see S. Datta 2006 *chapter 4 of Electron Transport in Mesoscopic Systems*, Cambridge University Press, Cambridge
- ³⁶ Qiao Z H, Wang J, Sun Q F, and Guo H, 2009 *Phys. Rev. B*, **79** 205308
- ³⁷ Sheng L, 2005 *Phys. Rev. Lett* **95** 136602
- ³⁸ Pan H, Li X, Jiang H, Yao Y G, and Yang S Y, 2015 *Phys. Rev B* **91** 045404
- ³⁹ Li X, Liu H W, Jiang H, Wang F, and Feng J 2012 *Phys. Rev. B*, **90** 165412
- ⁴⁰ Li D F and Shi J R 2009 *Phys. Rev. B* **79** 241303
- ⁴¹ Zhang Y Y, Shen M, An X T, Sun Q F, Xie X C, Chang K, and Li S S, 2014 *Phys. Rev. B*, **90**, 054205
- ⁴² Bernevig B A, Hughes T L and Zhang S C, 2006 *Science* **314** 1757
- ⁴³ Qi X L, Wu Y S, and Zhang S C, 2006 *Phys. Rev. B* **74** 085308
- ⁴⁴ Knez I, Du R -R, and Sullivan G, 2011 *Phys. Rev. Lett* **107** 136603
- ⁴⁵ Du L J, Knez I, Sullivan G, and Du R -R 2015 *Phys. Rev. Lett* **114** 096802
- ⁴⁶ Kane C L, 2008 *Nature Phys* **4** 348
- ⁴⁷ Guo H M, Lin Y and Shen S Q, 2014 *Phys. Rev. B* **115** 246603
- ⁴⁸ Fukui T, and Hatsugai Y, 2015 *J. Phys. Soc. Jpn*, **84** 043703
- ⁴⁹ Leeuw B d, Küpersbusch C, Juričić, and Fritz L, 2015 *Phys. Rev. B* **91** 235430
- ⁵⁰ Wang Z B, Song J T, Liu H W, Jiang H and Xie X C 2015 *New J. Phys.* **17** 113040
- ⁵¹ Zhu K, Wu L, Gong X X, Xiao S H, Li S Y, Jin X F, Yao M Y, Qian D, Wu M, Feng J, Niu Q, Juan F D, Lee D H, 2014 *arxiv* 1403.0066v1
- ⁵² Yao M Y, Zhu F F, Miao L, Han C Q, Yang F, Guan D D, Gao C L, Liu C H, Qian D, Jia J F, 2016 *Sci. Rep* **6** 21326
- ⁵³ Li J, Chu R L, Jain J K, and Shen S Q, 2009 *Phys. Rev. Lett* **102** 136806
- ⁵⁴ Guo H M, Rosenberg G, Refael G, and Franz M, 2009 *Phys. Rev. Lett* **105**, 216601.

- 55 Titum P, Lindner N H, Rechtsman M C, and Refael G 2015 *Phys. Rev. Lett* **114** 056801
- 56 Xing Y X, Zhang L, and Wang J 2011 *Phys. Rev. B*, **84** 035110
- 57 Xu D H, Gao J H, Liu C X, Sun J H, Zhang F C, and Zhou Y, 2014 *Phys. Rev. B*, **89** 195104
- 58 Hu L H, Xu, D H, Zhang F C, Zhou Y, 2016 *arxiv*: **1604.00821**
- 59 Qin W, Xiao D, Chang K, Shen S Q, and Zhang Z Y, 2015 *arxiv*: **1509.01666**
- 60 Borchmann J, Farrell A, and Pereg-Barnea T, 2016 *Phys. Rev. B* **93** 125133
- 61 Ryu S and Nomura K, 2012 *Phys. Rev. B* **85** 155138
- 62 Song J T, Prodan E, 2014 *Phys. Rev. B* **89** 224203
- 63 Song J T, Fine C, and Prodan E 2014 *Phys. Rev. B* **90** 184201
- 64 Orth C P, Sekera T, Bruder C, Schmidt T L 2016 *Sci. Rep* **6** 24007
- 65 Su Y, Avishai Y, Wang X R 2016 *arxiv*: **1601.02541**
- 66 Groth C W, Wimmer M, Akhmerov A R, Tworzydło J and Beenakker C W J, 2009 *Phys. Rev. Lett* **103** 196805
- 67 Bruus H, Flensberg K, 2004 *Many-body Quantum Theory in Condensed Matter Physics*, Oxford University Press
- 68 Song J T, Liu H W, Jiang H, Sun Q F, and Xie X C, 2012 *Phys. Rev. B* **85** 195125
- 69 Prodan E, 2011 *Phys. Rev. B* **83**, 195119
- 70 Xu D W, Qi J J, Liu J, Sacksteder V IV, Xie X C and Jiang H 2012 *Phys. Rev. B* **85** 195140
- 71 Zhang Y Y, Chu R L, Zhang F C, and Shen S Q 2012 *Phys. Rev. B* **85** 035107
- 72 Zhang Y Y, and Shen S Q 2012 *Phys. Rev. B* **88** 195145
- 73 Girschik A, Libisch F, and Rotter S. 2013 *Phys. Rev. B* **88**, 014201
- 74 Girschik A, Libisch F, and Rotter S. 2015 *Phys. Rev. B* **91**, 214204
- 75 Chen L, Liu Q, Lin X, Zhang X and Jiang X 2012 *New J. Phys.* **14** 043028
- 76 Weeks C, Hu J, Alicea J, Franz M, and Wu R, 2010 *Phys. Rev. X* **1** 021001
- 77 Hu J, Alicea J, Wu R, and Franz M 2012 *Phys. Rev. Lett* **109** 266801
- 78 Li Y C, Tang P Z, Chen P C, Wu J, Gu B L, Fang Y, Zhang S B, and Duan W H 2013 *Phys. Rev. B* **87** 245127
- 79 Qiao Z H, Yang S A, Feng W, Tse W K, Ding J, Yao Y, Wang J and Niu Q, 2010 *Phys. Rev. B* **82** 161414(R)
- 80 Ding J, Qiao Z, Feng W, Yao Y and Niu Q 2011 *Phys. Rev. B* **84** 195444
- 81 Zhang H, Lazo C, Blügel S, Heinze S, and Mokrousov Y, 2012 *Phys. Rev. Lett.* **108** 056802
- 82 Qiao Z H, Jiang H, Li X, Yao Y G, and Niu Q, 2012 *Phys. Rev. B* **85** 115439
- 83 Anderson P W, 1958 *Phys. Rev.* **109**, 1492
- 84 Abrahams E, Anderson P W, Licciardello D C, Ramkrishnan T V, 1979 *Phys. Rev. Lett.* **42** 673
- 85 Beenakker C W J, 1997 *Rev. Mod. Phys* **69** 731
- 86 Evers F and Mirlin A D 2008 *Rev. Mod. Phys.* **80** 1355
- 87 Huckestein B, 1995 *Rev. Mod. Phys* **67** 357
- 88 Chalker J T, and Coddington P D 1988 *J. Phys. C* **21** 2665
- 89 Slevin K and Ohtsuki T, 1997 *Phys. Rev. Lett.* **78** 4083
- 90 Onoda M, and Nagaosa N, 2003 *Phys. Rev. Lett* **90** 206601
- 91 Onoda M, Avishai Y, and Nagaosa N, 2007 *Phys. Rev. Lett* **98** 076802
- 92 Yamakage A, Nomura K and Imura K I, Kuramoto Y. 2011 *J. Phys. Soc. Jpn* **80**, 053703
- 93 Yamakage A, Nomura K and Imura K I, Kuramoto Y. 2013 *Phys. Rev. B* **87**, 205141
- 94 Obuse H, Furusaki A, Ryu S, and Mudry C, 2007 *Phys. Rev. B*, **76** 075301
- 95 Sbierski B, Pohl G, Bergholtz E J, and Brouwer P W, 2014 *Phys. Rev. Lett* **113** 026602
- 96 Sbierski B, Bergholtz E J, and Brouwer P W, 2015 *Phys. Rev. B* **92** 115145
- 97 Pixley J H, Goswami P, and Sarma S D, 2015 *Phys. Rev. Lett.* **115** 076601
- 98 Nielsen H B, and Ninomiya, 1981 *Nucl. Phys. B*, **185** 20
- 99 Yang K Y, Lu Y M, and Ran Y, 2011 *Phys. Rev. B* **84** 075129
- 100 MacKinnon A and Kramer B, 1981 *Phys. Rev. Lett* **47** 1546
- 101 Song J T, Prodan E, 2014 *Euro. Phys. Lett.* **105** 37001
- 102 Prodan E, 2011, *J. Phys. A*, **44** 113001
- 103 Liu S, Ohtsuki T, and Shindou R 2016 *Phys. Rev. Lett* **116** 066401
- 104 Shapourian H, and Hughes T L 2016 *Phys. Rev. B* **93** 075108
- 105 Bera S, Sau J D, and Roy B 2015 *arxiv*: **1507.07551v1**
- 106 Stü tzer S, Rechtsman M C, Titum P, Plotnik Y, Lumer Y, Zeuner J M, Nolte S, Refael G, Lindner N, Segev M, and Szameit A 2015 *Paper presented at CLEO: QELS Fundamental Science* 10.1364/CLEO_QELS.2015.FTh3D.2.
- 107 Liao J, Ou Y B, Feng X, Yang S, Lin C J, Yang W M, Wu K H, He K, Ma X C, Xue Q K, and Li Y Q, 2015 *Phys. Rev. Lett* **114** 216601
- 108 Nowack K C, Spanton E M, et al., 2013 *Nature Mater* **12** 787
- 109 Chen C Z, Liu H W, Jiang H, Sun Q F, Wang Z Q, and Xie X C, 2015 *Phys. Rev. B* **91** 214202
- 110 Qiao Z H, Wang K, Zhang L, Han Y L, Deng X Z, Jiang H, Yang S A, Wang J, Niu Q 2016 *arxiv* 1601.07367
- 111 Yu R, Zhang W, Zhang H J, Zhang S C, Dai X, and Fang Z, 2010 *Science* **329** 61
- 112 Soluyanov A A, Gresch D, Wang Z J, Wu Q S, Troyer M, Dai X, and Bernevig B A, 2015 *Nature*, **2015** 527
- 113 Liu H W, Jiang H, Sun Q F, and Xie X C, 2014 *Phys. Rev. Lett* **113** 046805